Turbulence, Heat and Mass Transfer 5
K. Hanjalić, Y. Nagano and S. Jakirlić (Editors)

DNS of Heat Transfer in a Transitional Channel Flow Accompanied by a Turbulent Puff-like Structure

T. Tsukahara[1], K. Iwamoto[1], H. Kawamura[1] and T. Takeda[2]

[1]*Department of Mechanical Engineering, Tokyo University of Science,*
Noda-shi, Chiba 278-8510, Japan, [*a7599109, iwamoto, kawa*]*@rs.noda.tus.ac.jp*

[2]*Nuclear Science and Engineering Directorate, Japan Atomic Energy Agency,*
Oarai-machi, Higashi Ibaraki-gun, Ibaraki 311-1393, Japan, takeda.tetsuaki@jaea.go.jp

Abstract — Direct numerical simulation of heat transfer in a fully developed channel flow has been carried out in a range of low Reynolds numbers from $Re_\tau = 180$ down to 60 (based on the friction velocity and the channel half width δ) with emphasis on a puff-like structure. For $Re_\tau \leq 80$ with the largest computational domain of $51.2\delta \times 2\delta \times 22.5\delta$, the turbulent puff is observed and significantly affects the momentum and heat transports. The spatial structure of the equilibrium puff is examined with taking account of two different thermal boundary conditions. It is revealed that there exists a localized strong turbulent region, in which a secondary flow is induced by the puff. In consequence, at the present lowest Reynolds number as low as $Re_\tau = 60$, the flow remains turbulent and the larger Nusselt numbers than those without puff is obtained.

1. Introduction

Heat transfer at a low Reynolds number Re in a turbulent/transitional channel flow is of practical importance with respect to a high temperature gas-cooled nuclear reactor, in which the low Re is employed to obtain a high outlet gas temperature with maintaining turbulence. Since the process of laminarization is also important in the field of both engineering applications and fundamental flow physics, the transition from turbulence to laminar has been studied experimentally by a number of researchers.

Direct numerical simulation (DNS) is a significant tool for the investigation of the turbulent heat transfer in a channel. The first such DNS was made by Kim and Moin [1] with an assumption of uniform heat generation at $Re_\tau = 180$, where Re_τ is based on the friction velocity u_τ and the channel half width δ. Lyons *et al.* [2, 3] performed the simulation at $Re_\tau = 150$ with the constant temperature difference boundary condition. At the same Reynolds number, Kasagi *et al.* [4] executed DNS in the case of uniformly heated walls. Later, the Reynolds- and Prandtl-numbers dependencies have been investigated by many research groups (e.g., Kawamura *et al.* [5, 6]). On the other hand, not much work has been done on DNS of heat transfer in a turbulent/transitional channel flow for a lower Reynolds number than $Re_\tau = 150$. This is because it requires a larger computational domain in order to capture an elongated streaky structure due to low Re. As for the transitional channel flow without a scalar transport, Iida and Nagano [7] carried out the DNS at $Re_\tau = 60$–100 to investigate the mechanisms of laminarization. The authors' group [8] showed that an isolated-turbulent structure (termed 'puff-like structure') was observed at $Re_\tau = 80$ by expanding the domain. The structure was found to be similar to the 'turbulent puff' in a transitional pipe flow studied by Wygnanski and Champagne [9].

Since most channel flows in various engineering systems can undergo laminar-to-turbulent transition below the critical Reynolds number given by the linear instability analysis, the subcritical transition in a channel flow has also been studied in many works. An early experimental study

Table 1: Reynolds numbers and domain box sizes of the present DNS: flow field with puff-like structure, ○; without puff, –. Bulk mean velocity, u_{m}; centerline mean velocity, u_{c}; box length in i-direction, L_i.

$Re_\tau\ (=u_\tau\delta/\nu)$	180	150	110	80	70	64	60†	80	64	60
$Re_{\mathrm{m}}\ (=u_{\mathrm{m}}2\delta/\nu)$	5680	4620	3270	2290	2000	1850	—	2310	1770	1640
$Re_{\mathrm{c}}\ (=u_{\mathrm{c}}\delta/\nu)$	3320	2710	1940	1400	1260	1200	—	1430	1140	1070
with/without Puff	—	—	—	—	—	—	—	○	○	○
Box size	Medium (MB)				Large (LB)			Extra-large (XL)		
$L_x \times L_y \times L_z$	$12.8\delta \times 2\delta \times 6.4\delta$				$25.6\delta \times 2\delta \times 12.8\delta$			$51.2\delta \times 2\delta \times 22.5\delta$		

† This case resulted in a laminarization.

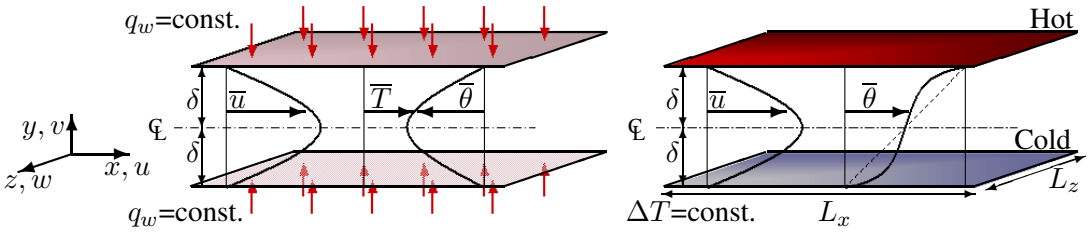

(a) Uniform heat-flux heating (cooling) (b) Constant temperature difference

Figure 1: Configurations of the thermal boundary conditions.

on the transitional channel flow was made by Davies & White [10]. Comparison of the existing experimental results indicates wide variation in the transitional Reynolds numbers. Patel & Head [11] obtained the transition Reynolds number of about $Re_{\mathrm{c}} = 1035$ with high-intensity disturbance in an inlet flow. Carlson *et al.* [12] made a flow-visualization study of turbulent spots with a smooth inlet in order to achieve a low-turbulence background flow. Their observations indicated that natural turbulent spots appeared spontaneously, leading to a transition at Re_{c} (defined in Table 1) slightly above 1000 as in Patel & Head [11]. These transitional Reynolds numbers are less than 20% of the critical Reynolds number ($Re_{\mathrm{c}} = 5772$) by the (two-dimensional) linear instability analysis [13]. Later, theoretical results of Orszag's group [14] inferred a transitional Reynolds number of about 1000, when finite-amplitude three-dimensional disturbance was considered.

These studies show the importance of nonlinear effects and of three-dimensional secondary instability associated with transitional structures, i.e. spots and puffs. Turbulent spots in a laminar channel flow have been studied extensively; turbulence characteristics inside a spot and its maintenance of turbulence are investigated in experiments by Klingmann & Alfredsson [15] and DNS by Henningson & Kim [16]. The structure of puffs in a transitional pipe flow was studied by Wygnanski's group [9, 17] and was found to be different from the structure of fully developed turbulent flow. In the transitional channel flow, the puff-like structure first observed by Tsukahara *et al.* [8], and this transitional structure must be significant for sustaining turbulence. To the knowledge of the authors, moreover, few numerical studies had focused on the effect of the transitional structure in a channel flow at turbulent-laminar transition range. Therefore it is necessary to know a mechanism of scalar transport in the puff-like structure with respect to enhancement of heat transfer.

Table 2: Computational box size; L_i, N_i and Δi^* (non-dimensionalized by δ) are a box length, a grid number and a spatial resolution of i-direction, respectively.

Box size	MB	LB	XL
$L_x \times L_y \times L_z$	$12.8\delta \times 2\delta \times 6.4\delta$	$25.6\delta \times 2\delta \times 12.8\delta$	$51.2\delta \times 2\delta \times 22.5\delta$
$N_x \times N_y \times N_z$	$512\times$ (96–128) $\times 256$	$512 \times 96 \times 256$	$1024 \times 96 \times 512$
$\Delta x^*, \Delta z^*$	0.05, 0.025	0.10, 0.05	0.05, 0.044
$\Delta y^*_{\rm min}$–$\Delta y^*_{\rm max}$	0.0011–0.033	0.0014–0.045	0.0014–0.045

In the present work, the various statistics associated with fully developed scalar fields for two different thermal boundary conditions are presented and discussed with emphasis on the role of the puff-like structure in the scalar transport. A series of DNS has been made for $Re_\tau = 60$–180 with the large computational box sizes as summarized in Tables 1 and 2.

2. Numerical procedure

The mean flow is driven by a uniform pressure gradient with passive scalar fields (see Figure 1). One of the thermal boundary conditions is the uniform heat-flux heating over the both surfaces (UHF), and the other is the constant temperature difference between the walls (CTD). The periodic boundary condition is imposed in the horizontal directions and the non-slip condition is applied on the walls. For the air of Prandtl number $Pr = 0.71$, all fluid properties are treated as constant. The fundamental equations are the continuity and the Navier-Stokes equations:

$$\frac{\partial u_i}{\partial x_i} = 0, \tag{1}$$

$$\frac{\partial u_i^+}{\partial t^*} + u_j^+ \frac{\partial u_i^+}{\partial x_j^*} = -\frac{\partial p^+}{\partial x_i^*} + \frac{1}{Re_\tau}\frac{\partial^2 u_i^+}{\partial x_j^{*2}} + \delta_{1i}, \tag{2}$$

where δ_{1i} corresponds to the mean pressure gradient. The energy equations are written as

$$\frac{\partial \theta^+}{\partial t^*} + u_j^+ \frac{\partial \theta^+}{\partial x_j^*} = \frac{1}{Re_\tau Pr}\frac{\partial^2 \theta^+}{\partial x_j^{*2}} + \frac{u^+}{u_{\rm m}^+} \quad \text{for UHF}, \tag{3}$$

$$\frac{\partial \Theta^+}{\partial t^*} + u_j^+ \frac{\partial \Theta^+}{\partial x_j^*} = \frac{1}{Re_\tau Pr}\frac{\partial^2 \Theta^+}{\partial x_j^{*2}} - v^+ \quad \text{for CTD}, \tag{4}$$

where in CTD, Θ ($= \theta/\Delta T - y^*$) is the deviation from the linear profile caused by the turbulence effect, and quantities with the superscript of $^+$ indicate those normalized by the wall variables and the friction temperature. The last terms on the right-hand side of Equations (3) and (4) represent a production by streamwise mean temperature gradient, $-u^+\partial_x T^+$, and a production by wall-normal temperature gradient of the linear profile, respectively. For the spatial discretization, the finite difference method is adopted. Further details of the numerical scheme can be found in Kawamura *et al.* [6]. Uniform grid mesh is used in the horizontal directions, and non-uniform mesh in the y direction. A coarser mesh ($N_y = 96$) is adopted for the low Reynolds numbers not over $Re_\tau = 80$. At $Re_\tau = 80$, the wall-normal grid spacings are $\Delta y^+ = 0.22$–3.59, which correspond to 0.13η–1.25η (η is referred to as a local Kolmogorov scale). These grid spacings are finer than ones used by Abe *et al.* [18], whose grid resolutions were approximately equal to 0.3η–1.6η.

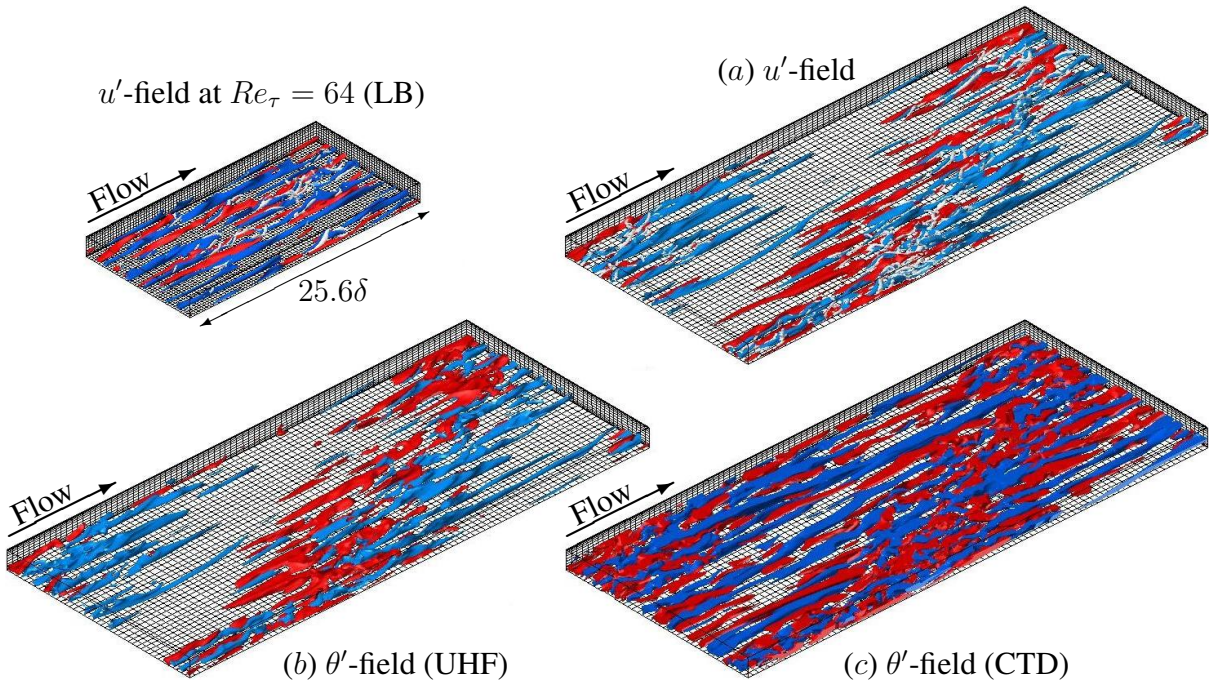

Figure 2: Instantaneous velocity and thermal fields for $Re_\tau = 64$ (XL): high/low-speed (a) and high/low-temperature (b, c) regions (red, u'^+, $\theta'^+ \geq 3.0$; blue, u'^+, $\theta'^+ \leq -3.0$). White isosurface in the flow field shows the contour of second invariant of the velocity gradient tensor: $I\!I'^+ = \partial u_i'^+/\partial x_j^+ \cdot \partial u_j'^+/\partial x_i^+ \leq -0.03$. The visualized volume is the lower half of the computational box, namely $51.2\delta \times \delta \times 22.5\delta$. A velocity field in the case of LB at the same Reynolds number is also shown for comparison.

A fully developed flow field at a higher Re is successively used as the initial condition for a one-step lower Re. Note that various statistical data and visualized fields are obtained after the scalar fields reached statistical-steady state. As for two-dimensional contours shown after, quasi-mean velocity and temperature statistics are temporally averaged for a time of $150\delta/u_\tau$ ($9600\nu/u_\tau^2$, 40 wash-out times). Further integration for $160\delta/u_\tau$ was necessary to obtain stable and accurate values of C_f and Nu presented here.

3. Results and Discussion

3.1. Instantaneous fields

The puff-like structure as mentioned in the introduction is observed in the present DNS at even lower Reynolds numbers than $Re_\tau = 80$. Figure 2(a) shows the instantaneous flow field accompanied by the turbulent puff, which is sustained and equilibrium for $Re_\tau = 60$–80 (XL). The quasi-streamwise vortices are well represented by the negative $I\!I'$ region, and the cluster of these fine-scale turbulent eddies is spatially isolated as seen in Figure 2(a). Note that the streaks elongated in the streamwise direction penetrate the computational domain in the case of LB, indicating a shortage of the box size. Moreover, fine-scale eddies are evenly distributed in the horizontal directions for LB. Flatness factors of the velocity fluctuations are affected significantly by expanding the box size (not shown here). Note also that in Figure 2, the computed equilibrium puff stays constant in size, whereas a turbulent spot in a laminar channel flow is known to be widely spread [19].

Turning now to Table 1 obtained from the present DNS, it will be seen that a turbulence (but spatially intermittent) is obtained at as low as $Re_{\rm c} = 1070$ ($Re_{\rm m} = 1640$), which is consistent with the experimental results [11, 12]. At this Reynolds number, turbulence is spatially intermittent, that is, coexistence of the turbulent puff-like structure and less turbulence in space. With decreasing Re, the intermittent flow is first observed at $Re_{\rm m} = 2300$ in the present DNS; on the other hand, an intermittent flow in an experiment occurs over the Reynolds number range $1380 < Re_{\rm m} < 1800$, cf. [11].

The isolated highly-disordered turbulent region, in which streaks are densely crowded, is spatially distributed in both x and z directions, while the turbulent puff of a pipe is intermittent only in the streamwise direction [9]. We have confirmed that this oblique structure in the channel flow was able to be captured even if an initial velocity field was a random distribution. Thus one may regard the inclination of the puff-like structure as essential for a transitional channel flow. As can be seen from Table 1, to capture the puff in a channel requires a large-scale domain such as XL. Neither MB nor LB is large enough for the equilibrium to become established. It is interesting to note that the self-sustaining puff in XL remains dominant with decreasing Re_τ from 64 to 60, while the turbulent flow has become laminar with LB.

From the visualization of the thermal fields affected by the puff, it is observed that thermal streaks in UHF (Figure 2(b)) are unevenly distributed and similar to the velocity field. This is attributed to similarity of the boundary conditions. In the cases of u' and θ' for UHF, the visualized iso-surfaces of negative fluctuation (blue color) show the low-speed (low-temperature) streaks in the wall region with an average spacing of 100 wall units. They are packed together and most are located at downstream of the highly-disordered turbulent region. In addition, this dense clustering of negative (also positive) fluctuations clearly exhibits a very large-scale pattern in the UHF field.

In the case of CTD, both high- and low-temperature regions tend to exist uniformly in the core region (see Figure 2(c)). Unlike UHF, the production of temperature variance for CTD is non-zero in the channel central region, and the location of maximum temperature variance is at the channel center. The thermal structure in the core region is dominant rather than the near-wall streak as seen from Figure 2(c). Thus, neither large-scale pattern nor the clustering of negative fluctuations is clearly observed in CTD with respect to puff-like structure. This will be discussed later.

3.2. Puff-like structure

3.2.1. Flow field

The puff-like structure emerges spontaneously from featureless turbulence: however, its oblique pattern is confined by the periodic boundary in both x and z directions, and parallels with a diagonal of the domain, as given in Figure 2. Accordingly, let us define z' as the coordinate which is parallel to the diagonal line. A value spatially-averaged in the z' direction and a fluctuation from this *quasi*-mean value are defined as:

$$\overline{u_i}^{z'}(x,y) = \frac{1}{T}\frac{1}{L_{z'}}\int_0^T\!\!\int_0^{L_{z'}} u_i(x+u_{\rm m}t, y, z', t)\mathrm{d}z'\mathrm{d}t, \quad u_i'' = u_i - \overline{u_i}^{z'}, \tag{5}$$

$$\overline{\theta}^{z'}(x,y) = \frac{1}{T}\frac{1}{L_{z'}}\int_0^T\!\!\int_0^{L_{z'}} \theta(x+u_{\rm m}t, y, z', t)\mathrm{d}z'\mathrm{d}t, \quad \theta'' = \theta - \overline{\theta}^{z'}. \tag{6}$$

Here, the propagation velocity of the puff was found, in the previous work [8], to be constant and almost equal to the bulk mean velocity $u_{\rm m}$. By assuming homogeneity of the puff in the z'

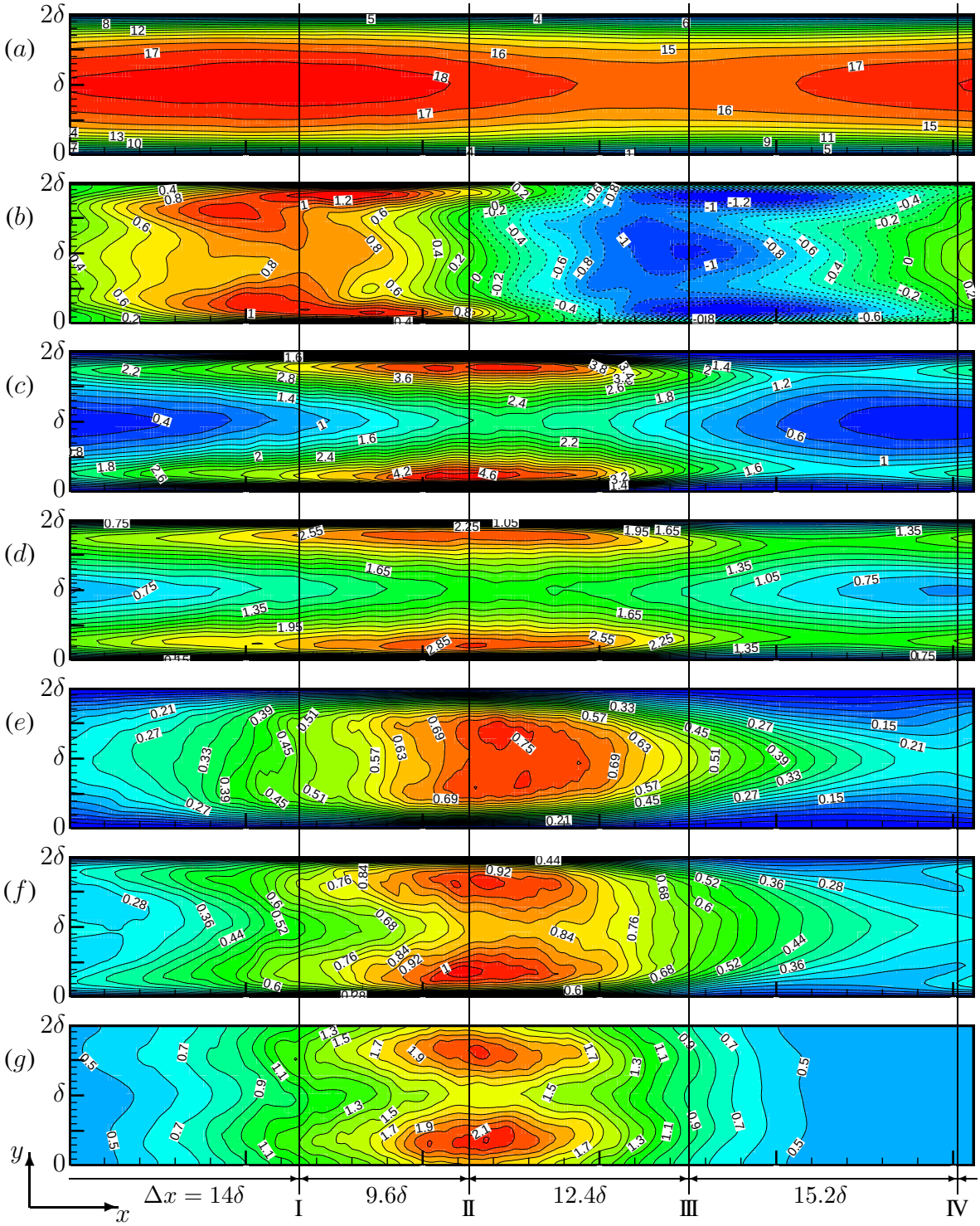

Figure 3 For legend see page 7.

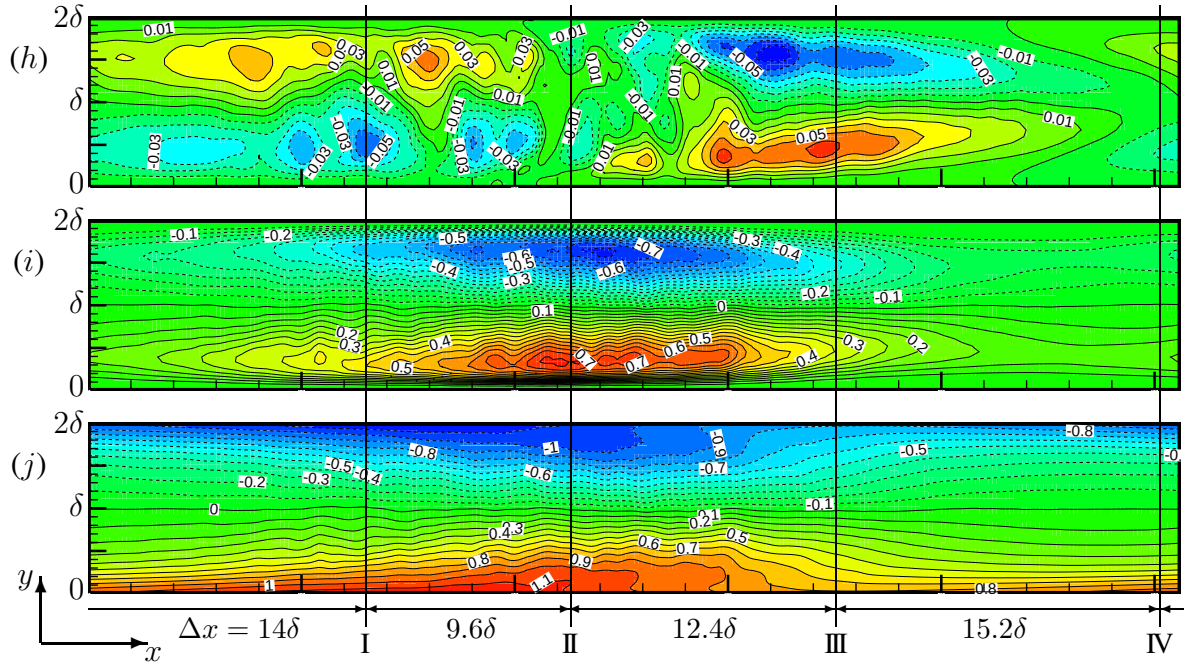

Figure 3: Quasi-mean flow field in an $(x$-$y)$ frame of reference moving with the puff at $Re_\tau = 64$ (XL): the ensemble-averaged pattern of (a) quasi-mean streamwise velocity $\overline{u}^{z'}$, (b) $\overline{u}^{z'} - \overline{u}$, (c) turbulent kinetic energy $k'' = \overline{u_i'' u_i''/2}^{z'}$, (d) turbulence intensity $u''_{\rm rms}$, (e) $v''_{\rm rms}$, (f) $w''_{\rm rms}$, (g) $p''_{\rm rms}$, (h) wall-normal component of quasi-mean velocity $\overline{v}^{z'}$, (i) Reynolds shear stress $-\overline{u''v''}^{z'}$, and (j) shear stress $\overline{\tau}^{z'}$ of Equation (7), where all of quantities are normalized by u_τ. Mean-flow direction is from left to right. Solid and dashed lines represent positive and negative quantities, respectively. The vertical lines are located at the streamwise locations where $\overline{u_{\rm c}}^{z'}$ is maximum (I) or minimum (Ⅲ); k'' maximum (Ⅱ) or minimum(Ⅳ).

direction, i.e. the direction from $(x, z) = (0, L_z)$ to $(L_x, 0)$ in Figure 2, the ensemble-averaged velocity and temperature fields with respect to the puff are obtained at $Re_\tau = 64$ (XL) as given in Figures 3–5. In these figures, one should keep in mind that the vertical scale is four times the abscissa scale. An overline of $\overline{(\cdot)}$ denotes the spatial (in both x and z directions) and temporal averaging.

Figure 3(b) shows that the large-scale regions of high- and low-speed fluctuations emerge occupying the whole width in the wall-normal direction. At the channel centerline, the quasi-mean velocity $\overline{u_{\rm c}}^{z'}$ becomes maximum (on the line I in Figure 3) about 22δ upstream from the position of minimum $\overline{u_{\rm c}}^{z'}$ (Ⅲ). This streamwise scale of the puff-like structure is almost same as that of an equilibrium puff in a transitional pipe (see, e.g., [20]). Between the upstream high-momentum (around the vertical-line I) and the downstream low-momentum regions (Ⅲ), an intensive-turbulence region (Ⅱ) appears as seen in Figure 3(c). On the other hand, around the line Ⅳ (called a 'region Ⅳ', hereafter), all the components of the turbulence intensity and the pressure fluctuation are attenuated as given in Figures 3$(d$–$g)$. Since the intensity of u'' is remarkably larger than those of the other two components, the contour of k'' (Figure 3(c)) resemble that of u''. The spatial extent of the reductions in k'' and u'' is coincided with the local acceleration of the mean flow in the region Ⅳ.

The quasi-mean v-velocity is as large as ± 0.05 just around the turbulent region (see Figure 3(h)), whereas in the fully turbulent channel flow the mean v must be zero. The high-

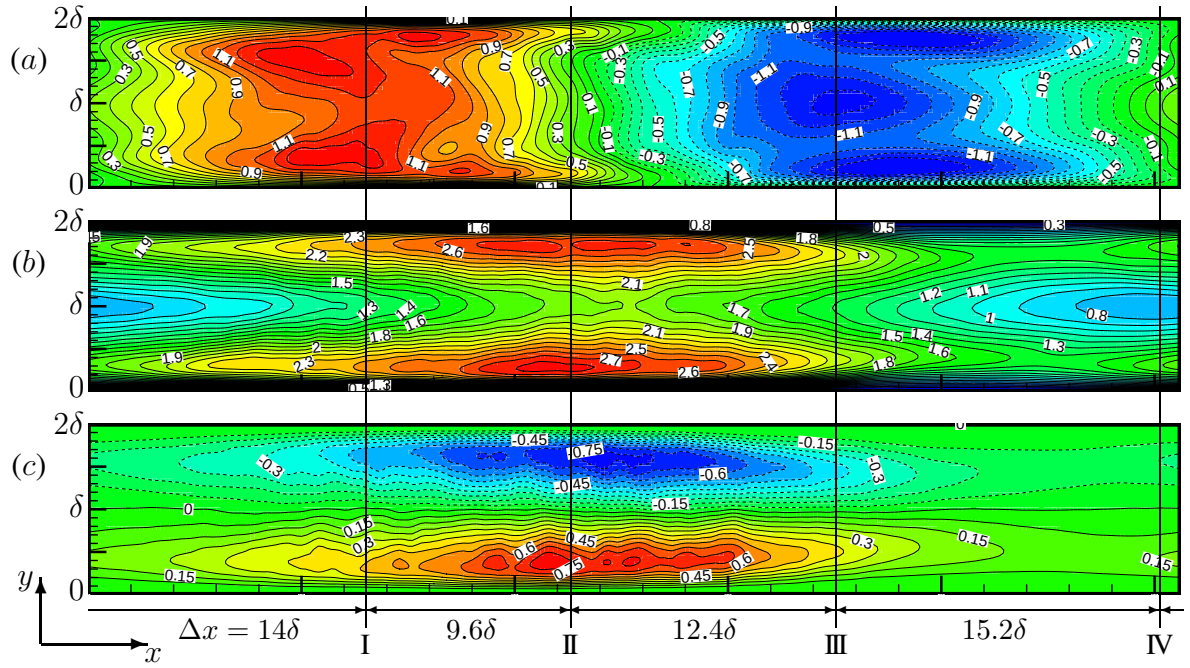

Figure 4: Quasi-mean thermal field of UHF in an (x-y) frame of reference moving with the puff at $Re_\tau = 64$ (XL): the ensemble-averaged pattern of (a) deviation between *quasi*-mean and mean temperature ($\overline{\theta}^{z'} - \overline{\theta}$), ($b$) temperature variance $\theta''_{\rm rms}$, and (c) wall-normal turbulent heat flux $-\overline{v''\theta''}^{z'}$, where all of quantities are normalized with a friction temperature (and a friction velocity). Mean-flow direction is from left to right. Solid and dashed lines represent positive and negative quantities, respectively. Positions of the vertical lines with the numerals I–IV are same as those in Figure 3.

momentum fluid (around I of Figure 3(b)) impinges on the downstream low-momentum one and is swept towards the walls in the upstream extent of the interface, ∼I∼II. On the contrary, one can observe that the fluid converges towards the channel center as it crosses the interface II∼III∼.

The contours of the Reynolds shear stress and total one (defined by the following equation) are shown in Figures 3(i) and (j), respectively.

$$\overline{\tau}^{z'} = -\overline{u}^{z'}\overline{v}^{z'} - \overline{u''v''}^{z'} + \nu\frac{\partial \overline{u}^{z'}}{\partial y}. \tag{7}$$

Here, $-\overline{u}^{z'}\overline{v}^{z'}$ is very small compared to $-\overline{u''v''}^{z'}$, so that $-\overline{u}^{z'}\overline{v}^{z'}$ is neglected here. A fully turbulent channel flow is homogeneous in the horizontal directions, so that the all derivatives with respect to x and z can be assumed to be zero, except for the pressure gradient $\partial_x\overline{p}$, which drives the mean flow, cf. [21]. On the other hand, the flow with the puff is homogeneous only in the z' direction, so that the total shear stress is not strictly defined as Equation (7). However, all derivatives with respect to x and z (not shown here) are small enough compared to the terms of Equation (7). The maximum Reynolds stress is located at about $y = 0.4\delta$ in the region II , where the secondary flow appears with significant non-zero $\overline{v}^{z'}$. Even though $\overline{v}^{z'}$ is small, its effect on the velocity $\overline{u}^{z'}$ at the near-wall region is large. In consequence, the wall shear stress (and the skin friction coefficient) changes about 40% in the streamwise direction.

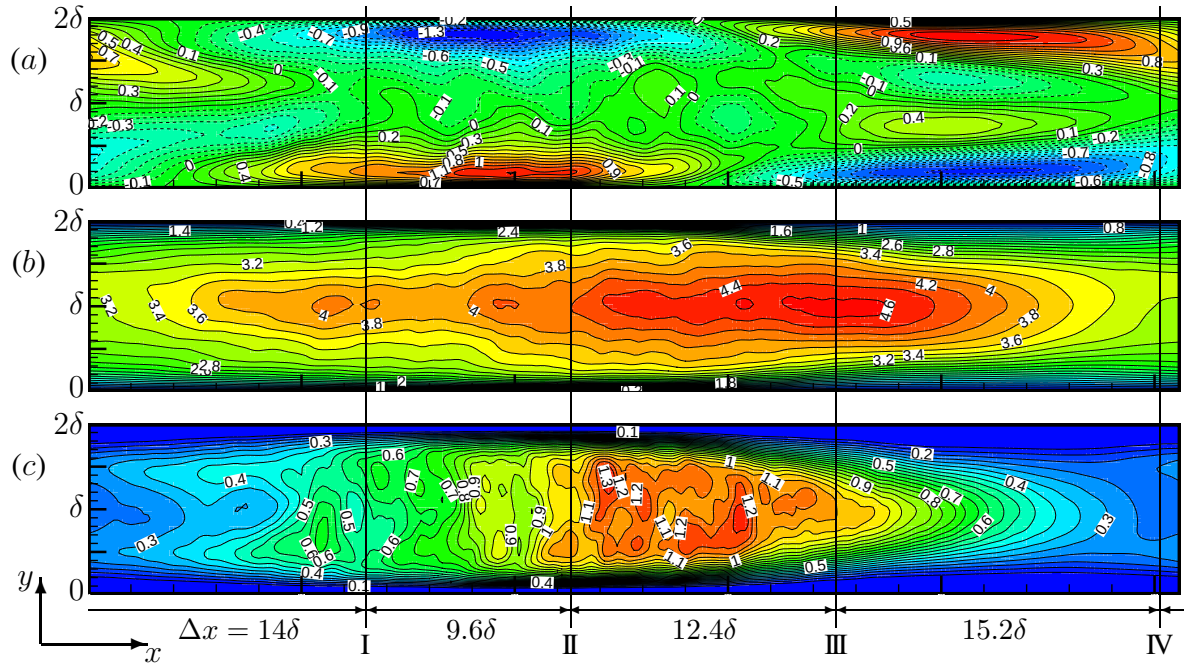

Figure 5: Same as Figure 4 but for CTD.

3.2.2. Thermal fields

Using Equation (6), the averaged properties for the thermal fields of UHF and CTD are given in Figures 4 and 5, respectively. Figure 4(a) shows the contour of the quasi-mean temperature for UHF, indicating the existence of large-scale structure (high- and low-$\overline{\theta}^{z'}$ regions) similar to that of the velocity field shown in Figures 3(b). On the other hand, such structure cannot be found in the case of CTD (Figure 5(a)). Also shown in Figures 4(b) and 5(b) are the root-mean-square fluctuations $\theta''_{\rm rms}$ for each temperature fields. The difference in the distributions of $\theta''_{\rm rms}$ between the two thermal boundary conditions results from the difference in each distribution of $\overline{v''\theta''}^{z'}$. Figure 4($c$) shows the contour of $\overline{v''\theta''}^{z'}$ for UHF; it displays intermittent regions of large $\overline{v''\theta''}^{z'}$ similar to the spatial distribution of $\overline{u''v''}^{z'}$. This implies that strong production of the scalar fluctuation also takes place intermittently just as that of the velocity fluctuation. As for CTD, the intermittent distribution of $\overline{v''\theta''}^{z'}$ is clearly identified but large $\overline{v''\theta''}^{z'}$ is located at the channel center and slightly downstream from the line Ⅱ, as given in Figure 5(c). Both Figures 4(c) and 5(c) indicate that around the line Ⅱ, the wall-normal heat flux becomes as large as twice of its mean values (not shown here) in both of the thermal boundary conditions. This spatial intermittency of the effective heat transport is associated with the wall-normal secondary flow (see Figure 3(h)). The flow pattern of the secondary flow is symmetric about the channel centerline whereas the wall-normal mean temperature profile of CTD is asymmetric. Hence a streamwise variation of $\overline{\theta}^{z'}$ is negligible at the channel center as seen from Figure 5(a). As a result, no large-scale structure of θ' for CTD is found in the visualization shown in Figure 2(c). In the near-wall region, however, Figure 5(a) shows significant variation of $\overline{\theta}^{z'}$ in the x direction, see also Figure 4(a) for UHF. The wall heat flux $\overline{q_{\rm wall}}^{z'} (= \partial_y \overline{\theta}^{z'})$ also changes about 60% in the x direction for both thermal boundary conditions. This reveals that heat transfer (and, therefore, Nusselt number) is spatially enhanced by the puff.

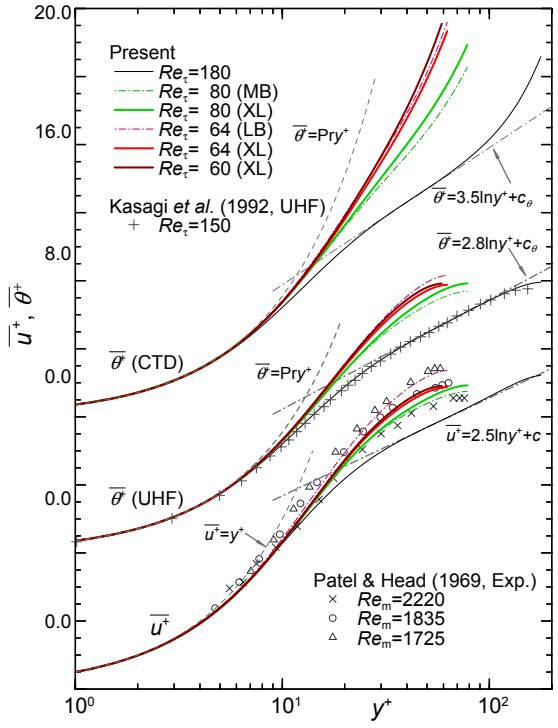

Figure 6: Mean velocity $\overline{u}$ and temperature $\overline{\theta}$ profiles in viscous wall-units.

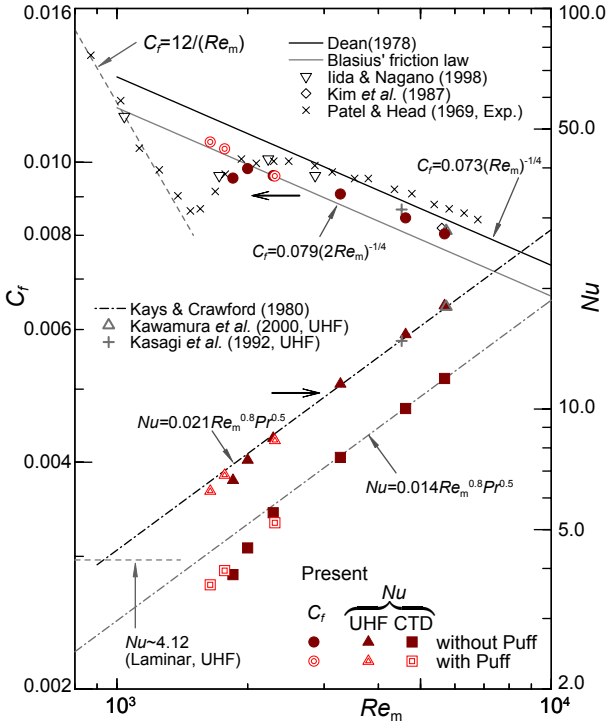

Figure 7: Variation with Reynolds number of C_f and Nu. Laminar flow relations, (– – –).

3.3. Mean flow parameter

The dimensionless mean velocity and temperature profiles are shown in Figure 6. For $Re_\tau \leq 80$, the Reynolds-number dependence of the mean velocity profile in the present DNS data is consistent with that by Patel & Head [11]. The friction Reynolds number of the experiment was set to be $Re_\tau = 59$–77. If emphasis is placed on the data at $Re_\tau = 80$ (MB and XL), the profiles suggest that the maximum (channel-centerline) values of $\overline{u}^+$ and $\overline{\theta}^+$ increase with extending the box size up to XL, since the quasi-laminar region locally appeared in the flow field. However, the Reynolds-number dependencies of both mean velocity and temperature profiles in the flow involving the puff are significantly smaller than those without the puff. For instance, the centerline velocity $\overline{u_c}^+$ is almost unchanged (or decreased 0.5%) with decreasing Re_τ from 80 to 64 in the case of XL, whereas increased by about 7% between $Re_\tau = 80$ (MB) and 64 (LB), in which puff does not take place.

Figure 7 shows variations of the skin friction coefficient C_f and the Nusselt number Nu in comparison with the empirical correlations for a turbulent flow, together with the experimental data. They are non-dimensionalized in the present definition as

$$C_f = \frac{\tau_{\rm wall}}{\frac{1}{2}\rho u_{\rm m}^2} = \frac{2}{u_{\rm m}^{+2}}, \quad Nu = \frac{h \cdot 2\delta}{\lambda} = \frac{2Re_\tau Pr}{\theta_{\rm m}^+}, \tag{8}$$

where $\tau_{\rm wall}$, ρ, $\theta_{\rm m}$, λ and h are the averaged wall shear stress, the density, the bulk mean temperature, the thermal conductivity and the heat transfer coefficient, respectively. The wall shear stress and heat transfer are locally enhanced by the puff-like structure as indicated already. As a result, both of C_f and Nu with the puff tend to be slightly higher than those without puff, and stay closer to the empirical correlations even for very low Reynolds numbers.

4. Conclusions

We performed DNS of turbulent heat transfer in a transitional channel flow with two different thermal boundary conditions down to $Re_\tau = 60$, and investigated the characteristics of the flow and thermal fields accompanied by a puff-like structure (called 'puff', hereafter).

The puff occurs over the Reynolds-number range $Re_\tau \leq 80$ ($Re_\mathrm{m} \leq 2300$, or $Re_\mathrm{c} \leq 1430$) with the computational domain of $(L_x \times L_z) = (51.2\delta \times 22.5\delta)$. The puff maintains the intermittent turbulence as low as $Re_\tau = 60$ ($Re_\mathrm{m} = 1640$, or $Re_\mathrm{c} = 1070$), whereas the flow without the puff becomes laminar at the larger Re ($Re_\tau = 60$–64) than the transitional Reynolds number obtained in experiments [11, 12]. The puff oblique with respect to x and z directions is observed to emerge from an initial random distribution, although the influence of the periodic boundary condition cannot be neglected. The homogeneous direction of the puff is tilted at an angle of $\tan^{-1}(L_z/L_x)$ ($= 24^\circ$ in this case) to the x direction. The turbulent and heat transfer properties of the puff are investigated. It is revealed that the secondary flow around the laminar-turbulent interface induces the isolated strong-turbulence region. The streaky structure usually found in fully developed turbulent flows are also present in the intermittent-turbulence part of the puff. In consequence, an localized large C_f and Nu region occurs; moreover, their ensemble-averaged values are significantly larger than those without puff for $Re_\tau \leq 64$.

Acknowledgements

The present study is entrusted from Ministry of Education, Culture, Sports, Science and Technology of Japan, and the first author (T. Tsukahara) is supported by Japan Society for the Promotion Science (JSPS) Fellowship. The present computations were performed with use of the supercomputing resources at Information Synergy Center of Tohoku University.

References

1. J. Kim and P. Moin, Transport of passive scalars in a turbulent channel flow. In *Turbulent Shear Flows 6* (*Edited by J.-C. André*), pp. 85–96, Springer-Verlag, Berlin, 1989.
2. S. L. Lyons, T. J. Hanratty and J. B. Mclaughlin, Large-scale computer simulation of fully developed turbulent channel flow with heat transfer. *Int. J. Num. Method in Fluids*, 13: 999–1028, 1991.
3. S. L. Lyons, T. J. Hanratty and J. B. Mclaughlin, Direct numerical simulation of passive scalar heat transfer in a turbulent channel flow. *Int. J. Heat and Mass Transfer*, 39: 1149–1161, 1991.
4. N. Kasagi, Y. Tomita and A. Kuroda, A direct numerical simulation for passive scalar field in a turbulent channel flows. *Trans. ASME* C: *J. Heat Transfer*, 114: 598–606, 1992.
5. H. Kawamura, K. Ohsaka, H. Abe and K. Yamamoto. DNS of turbulent heat transfer in channel flow with low to medium-high Prandtl number fluid. *Int. J. Heat and Fluid Flow*, 19: 482–491, 1998.
6. H. Kawamura, H. Abe and K. Shingai. DNS of turbulence and heat transport in a channel flow with different Reynolds and Prandtl numbers and boundary conditions. In *Third International Symposium on Turbulence, Heat and Mass Transfer* (*Edited by Y. Nagano, K. Hanjalic and T. Tsuji*), pp. 15–32, 2000.
7. O. Iida and Y. Nagano. The relaminarization mechanisms of turbulent channel flow at low Reynolds numbers. *Flow, Turbulence and Combustion*, 60: 193–213, 1998.
8. T. Tsukahara, Y. Seki, H. Kawamura and D. Tochio. DNS of turbulent channel flow at

very low Reynolds numbers. In *Fourth International Symposium on Turbulence and Shear Flow Phenomena* (*Edited by J. A. C. Humphrey et al.*), pp. 935–940, 2005.

9. I. J. Wygnanski and F. H. Champagne. On transition in a pipe. Part 1. The origin of puffs and slugs and the flow in a turbulent slug. *J. Fluid Mech.*, 59: 281–335, 1973.
10. S. J. Davies and C. M. White. An experimental study of the flow water pipes of rectangular section. *Proc. R. Soc. Lond.*, A 119: 92–107, 1928.
11. V. C. Patel and M. R. Head. Some observations on skin friction and velocity profiles in fully developed pipe and channel flows. *J. Fluid Mech.*, 38: 181–201, 1969.
12. D. R. Carlson, S. E. Widnall and M. F. Peeters. A flow-visualization study of transition in plane Poiseuille flow. *J. Fluid Mech.*, 121: 487–505, 1982.
13. S. A. Orszag. Accurate solution of the Orr Sommerfeld stability equation. *J. Fluid Mech.*, 50: 689–703, 1971.
14. S. A. Orszag and L. C. Kells. Transition to turbulence in plane Poiseuille flow and plane Couette flow. *J. Fluid Mech.*, 96: 159–205, 1980.
15. B. G. B. Klingmann and H. Alfredsson. Turbulent spots in plane Poiseuille flow – Measurements of the velocity field. *Phys. Fluids*, A2: 2183–2195, 1990.
16. D. S. Henningson and J. Kim. On turbulent spots in plane Poiseuille flow. *J. Fluid Mech.*, 228: 183–205, 1991.
17. I. J. Wygnanski, M. Sokolov and D. Friedman. On transition in a pipe. Part 2. The equilibrium puff. *J. Fluid Mech.*, 69: 283–304, 1975.
18. H. Abe, H. Kawamura and Y. Matsuo. Direct numerical simulation of a fully developed turbulent channel flow with respect to the Reynolds number dependence. *Trans. ASME* I: *J. Fluids Engng.*, 123: 382–393, 2001.
19. D. S. Henningson, P. Spalart and J. Kim. Numerical simulations of turbulent spots in plane Poiseuille and boundary-layer flow. *Phys. Fluids*, 30: 2914–2917, 1987.
20. V. G. Priymak and T. Miyazaki. Direct numerical simulation of equilibrium spatially localized structures in pipe flow. *Phys. Fluids*, 16: 4221–4234, 2004.
21. H. Tennekes and J. L. Lumley. In *A first course in turbulence*, MIT Press, Cambridge, MA, 1972.
22. R. D. Dean. Reynolds number dependence of skin friction and other bulk flow variables in two-dimensional rectangular duct flow. *Trans. ASME* I: *J. Fluids Engng.*, 100: 215–222, 1978.
23. W. M. Kays and M. E. Crawford. In *Convective heat and mass transfer*, 2nd ed., McGraw-Hill, New York, 1980.